Full Length Article

Specimen aspect ratio and progressive field strain development of sandstone under uniaxial compression by three-dimensional digital image correlation

H. Munoz [a,b,*], A. Taheri [b]

[a] Deep Exploration Technologies Cooperative Research Centre (DET CRC), Export Park, Adelaide Airport, Adelaide, SA 5950, Australia
[b] School of Civil, Environmental & Mining Engineering, The University of Adelaide, Adelaide, SA 5005, Australia

ABSTRACT

The complete stress–strain characteristics of sandstone specimens were investigated in a series of quasi-static monotonic uniaxial compression tests. Strain patterns development during pre- and post-peak behaviours in specimens with different aspect ratios was also examined. Peak stress, post-peak portion of stress–strain, brittleness, characteristics of progressive localisation and field strain patterns development were affected at different extents by specimen aspect ratio. Strain patterns of the rocks were obtained by applying three-dimensional (3D) digital image correlation (DIC) technique. Unlike conventional strain measurement using strain gauges attached to specimen, 3D DIC allowed not only measuring large strains, but more importantly, mapping the development of field strain throughout the compression test, i.e. in pre- and post-peak regimes. Field strain development in the surface of rock specimen suggests that strain starts localising progressively and develops at a lower rate in pre-peak regime. However, in post-peak regime, strains increase at different rates as local deformations take place at different extents in the vicinity and outside the localised zone. The extent of localised strains together with the rate of strain localisation is associated with the increase in rate of strength degradation. Strain localisation and local inelastic unloading outside the localised zone both feature post-peak regime.
© 2017 Institute of Rock and Soil Mechanics, Chinese Academy of Sciences. Production and hosting by Elsevier B.V. This is an open access article under the CC BY-NC-ND license (http://creativecommons.org/licenses/by-nc-nd/4.0/).

1. Introduction

The characterisation of post-peak behaviour associated with the decrease of rock load-bearing capacity, crack development as well as rock brittleness is critical to many civil engineering applications, mining development projects, and mineral exploration operations. The complete stress–strain characteristics of intact rock, i.e. pre- and post-peak regimes, picture the total process of rock deformation and failure behaviour. Pioneering studies on the complete stress–strain behaviour of rocks undergoing quasi-static compression basically classify rocks into two categories (Wawersik and Fairhurst, 1970; Hudson et al., 1971; Wawersik and Brace, 1971; Fairhurst and Hudson, 1999): class I, which is characterised by a negative post-peak slope, where fracture propagation is controllable by a rigid

axial-displacement controlled machine, and class II, showing positive post-peak slope, where fracture propagation is uncontrollable using the same testing arrangement. The failure mechanism of brittle rocks generally has a noticeable display of abrupt post-peak drop in stress immediately after the peak strength takes place towards the residual strength, if any, on the characteristic stress–strain curve (Wawersik and Fairhurst, 1970; Wawersik and Brace, 1971; Martin and Chandler, 1994). The determination of this abrupt drop of stress has been a key issue relevant to a number of geotechnical engineering applications, including for instance unstable behaviour analysis of brittle-plastic rock mass in large rock excavations, and it has been approached by extending the classical theory of plasticity to modelling brittle-plastic materials (Zheng et al., 2005).

Rock behaviour under axial loading is generally studied in laboratory using load- or displacement-controlled compressive loading systems. Load-controlled method, however, can only measure pre-peak behaviour. A common method to control axial load is to use axial displacement (or axial strain) rate feedback in servo-controlled compressive machines (Bieniawski and Bernede,

* Corresponding author.
  E-mail address: henry.munozprincipe@adelaide.edu.au (H. Munoz).

1979). To measure the post-peak behaviour of rocks, this method has been used in unconfined and confined conditions (e.g. Gowd and Rummel, 1980; Taheri and Tani, 2008; Kumar et al., 2010; Taheri et al., 2016). Nevertheless, axial strain feedback is insufficient to measure post-peak regime for class II rocks. This is because axial strain in the compression tests no longer increases monotonically from the moment rock starts behaving as class II (Munoz et al., 2016a). As a result, using axial-strain feedback method, a critical response on the rock stress–strain curve takes place, suggesting rock drastic failure. Consequently, post-peak stress–strain behaviour is masked by a rapid strength reduction at constant axial displacement immediately after peak stress (e.g. Labuz and Biolzi, 2007). However, this post-peak critical response may be a manifestation of axial displacement-controlled machine compliance, but not material behaviour. Circumferential- or lateral-strain controlled method, however, is suggested to measure post-peak stress–strain for brittle rocks. This is mainly because lateral displacement monotonically increases after the peak stress even if axial displacement decreases (Munoz et al., 2016a).

Not only the proper application and correct measurement of load, but also the proper measurement of deformations and strains in the specimen are crucial to obtain features of stress–strain in pre- and post-peak regimes. The latter can be accomplished by instant deformations of the material provided by a series of digital images. Digital image correlation (DIC) technique refers to the class of non-contact deformation and motion measurement method, recording simultaneous image points of undeformed and deformed states of an object (Sutton et al., 2009). Two-dimensional (2D) DIC has been previously employed in material deformation measurement under predominantly in-plane displacements and strains conditions (Dautriat et al., 2011; Nguyen et al., 2011). However, 2D DIC is impractical to be applied to cylindrical specimens in uniaxial compression as relatively small out-of-plane motions introduce errors in the measurement of in-plane displacements. Three-dimensional (3D) DIC solves the limitations of 2D DIC as 3D DIC method allows full-field 3D shape and displacement measurements.

There are few investigations on the field strain pattern development of rocks under uniaxial compression in pre- or post-peak regimes using 3D DIC technique. Therefore, non-contact strain measurement via 3D DIC becomes relevant to measuring the field of strains development in post-peak regime. In addition, this technique has rarely been implemented to study effect of specimen aspect ratio (i.e. length to diameter ratio) on rock strain pattern development in pre- and post-peak regimes during uniaxial compression.

2. Experimental study

A series of uniaxial compression tests was carried out on Hawkesbury sandstone. Compression tests complied with lateral-strain controlled method in order to obtain the post-peak behaviour of rock. To study the aspect ratio and its effect on the development of strain patterns, together with pre- and post-peak stress–strain characteristics, a number of rock specimens were tested herein, having aspect ratios of 1.5, 2.4 and 3.5.

Sections below describe in detail the steps for rock preparation and instrumentation, the application of 3D DIC technique to measure deformation, and the lateral-strain controlled loading method. Features and limitations of other loading control methods, including axial-strain and axial-load, are discussed in Section 3.

2.1. Rock material and preparation

Hawkesbury sandstone is an early Middle Triassic rock abundant in New South Wales, Australia. Hawkesbury sandstone is fine-grained and has a dry density of 2260 kg/m^3.

The rock was quarried and then prepared into blocks. Later the blocks were cored for cylindrical specimens. The diameter of specimens was 42 mm. A visual inspection showed that the specimens diameter was from 10 to more than 20 times larger than the rock grains size recommended by the International Society for Rock Mechanics (ISRM) (Bieniawski and Bernede, 1979; Fairhurst and Hudson, 1999). The end faces and sides of the specimen were prepared smooth and straight according to the ISRM standard (ISRM, 1981; Fairhurst and Hudson, 1999).

2.2. Rock instrumentation

Axial deformation of the specimens was measured externally by a pair of axial linear variable displacement transducers (LVDTs) mounted on both left and right sides of specimen. Axial strains ε_A were calculated from the LVDTs readings. In addition, the rock specimen was instrumented with a direct-contact lateral extensometer (i.e. lateral ring-shaped extensometer) which was wrapped around the cylindrical specimen. This device was essential to control the axial load by lateral strain feedback. Fig. 1 shows the arrangement of LVDTs and lateral extensometer in a rock specimen.

The lateral extensometer was mounted at the mid-length of the specimens so that end-edge friction effects (Hawkes and Mellor, 1970) of confined zones due to boundary conditions (van Vliet and van Mier, 1995) on the measurements were eliminated. Lateral strains ε_L were calculated from the change in diameter of specimen induced by axial load. The lateral extensometer type used in the tests was 632.12F20-series manufactured by MTS Systems Co.

2.3. 3D DIC method

Typical testing using 2D DIC requires predominantly in-plane displacements and strains, assuming that the specimen is planar and deformation is within the object plane. 2D DIC technique encompasses the use of a single digital camera positioned opposite to the surface of the specimen. Since in-plane motions are assumed to occur in two dimensions, calibration is performed with planar motions. 2D DIC results are impractical to be applied to rock cylinders in uniaxial compression, since, in this particular case, in-plane motions are no longer applicable to curved surfaces.

3D DIC solves the limitations of 2D DIC. 3D DIC technique encompasses the use of two digital cameras positioned in a manner that ensures the surface of the specimen to be viewed from two different angles, which allows full-field 3D shape and displacement measurements (i.e. recovering the 3D position).

The aforementioned can be explained by Fig. 2 (Sutton et al., 2009). In this figure, by using a single camera, two 3D points Q and R are imaged onto a single image point p, which demonstrates that the image point p corresponds to infinite 3D points. In contrast, by using two cameras to record the image points of the same object simultaneously, a unique 3D point Q corresponds to image points (p, q'). Similarly, the image point (p, r') corresponds to a unique 3D point R.

Rock surface deformations induced by the compressive load throughout the tests were captured by taking a significant number of images of the speckle surface of the specimens by using a couple of digital cameras (i.e. Fujinon HF75SA-1, 1:1.8/75 mm, 5 megapixels resolution) suitable for quasi-static loading tests. The speckle pattern on the rocks was created by first spraying ordinary white paint and then by tarnishing black paint.

The speckle pattern was non-repetitive, isotropic and high in contrast, i.e. random pattern exhibiting no bias to an orientation and showing dark black and bright white, which were adequate in size for high strain resolution (Sutton et al., 2009). Prior to the
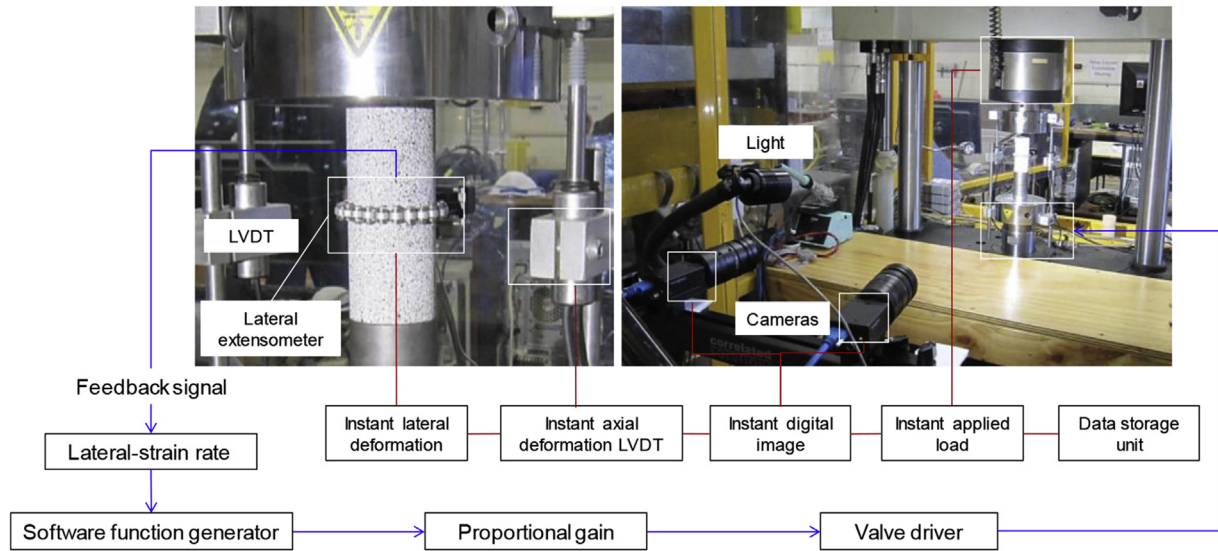
Fig. 1. Experimental set-up: servo-controlled closed-loop testing system and two-camera stereo system for 3D DIC in uniaxial compression.

compression tests, each camera was calibrated using a 30-mm standard target having uniformly spaced markers (see Fig. 3). After calibration, the standard deviation of residuals was 0.02 (in pixel). This value suggests that the calibration of the cameras is adequate

for the measurement (Sutton et al., 2009). More details can be found in Munoz et al. (2016b).

In compliance with lateral strain control used in the tests, the axial displacement and axial loading rate before the peak stress are relatively high. Conversely, after peak stress takes place, the axial load is applied at a slower rate (i.e. a load rate from 10 to 100 times slower) to keep the lateral strain rate constant. Therefore, images of deformed states of the specimen were captured at a frame rate of an

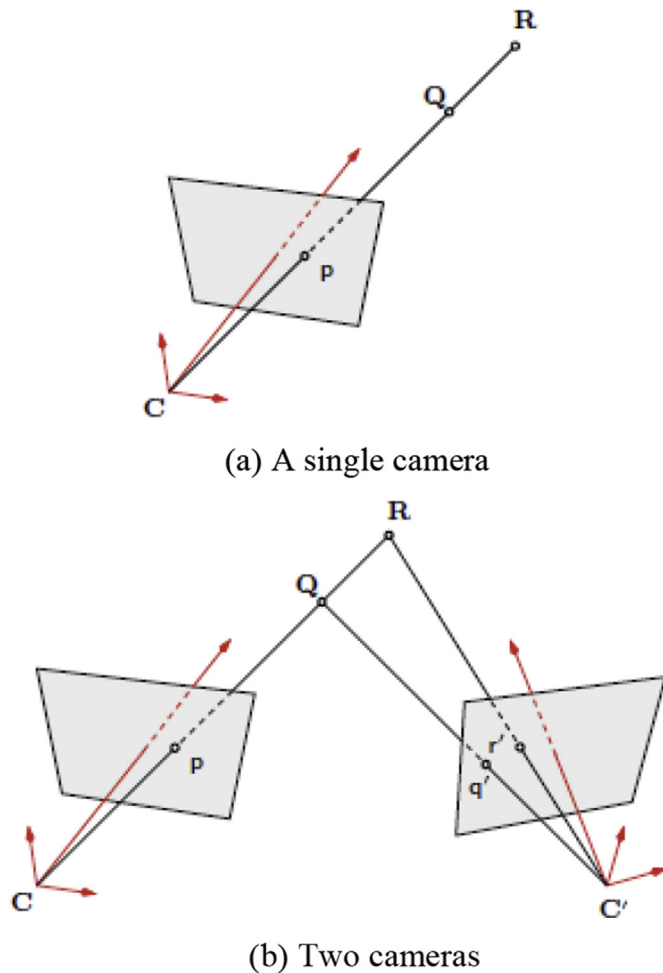(a) A single camera

(b) Two cameras

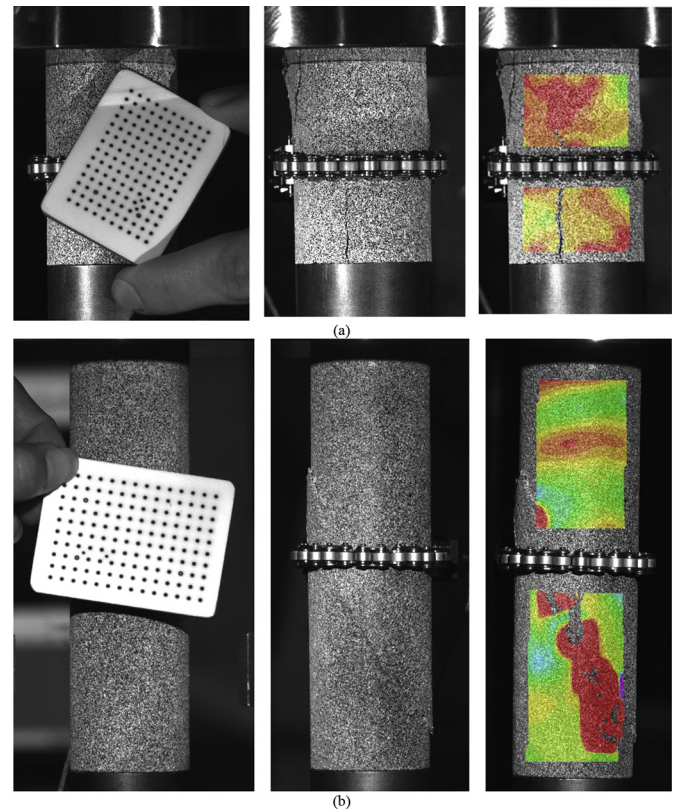Fig. 2. (a) A single and (b) two cameras for recovering the third dimension (Sutton et al., 2009).

Fig. 3. Calibration procedure for the stereo cameras and rock specimens at the end of the compression tests (i.e. $q \approx 0.07q_{peak}$; where q is the axial stress and q_{peak} is the peak axial stress) along with axial field of strains by 3D DIC for specimens with aspect ratios of (a) 1.5 and (b) 3.5.

image each 0.5 s, from the start of loading for the first 30 min (time enough to reach peak stress), and thereafter an image each 5 s until the end of the tests (throughout the post-peak regime). The aforementioned time frame arrangement for capturing images was suitable to track deformations throughout pre- and post-peak regimes by a large number of images, about 6000 pictures captured in total. Images of undeformed (reference state) and deformed states of the specimen were captured automatically by Vic-Snap software.

Instantaneous axial deformation, lateral deformation, applied load and instantaneous images were synchronously acquired to ensure one-to-one correspondence between load, deformation and respective images. Imaging data processing for deformations and strains was conducted by VIC-3D software (Sutton et al., 2009). Deformations and strains were always obtained by comparing the reference image (undeformed state) with subsequent images of the rock deforming after load was applied.

A portion of the surface of the rock was captured and analysed under 3D deformation (see Fig. 3), i.e. the area of interest. 3D deformations taking place behind the area of interest were not able to be captured under the present arrangement (i.e. by a couple of digital cameras). To do so, at least three sets of cameras (a couple of cameras for each set) surrounding the specimen will be needed. 3D DIC tests were repeated several times in order to capture the typical failure pattern (i.e. axial cracks or shear plane) of specimens within the area of DIC measurement.

2.4. Loading set-up and testing method

The rock specimens were subjected to a quasi-static monotonic axial loading by a compressive machine which was stiff enough not to allow the elastic energy accumulated in the machine (i.e. Instron-1342 model manufactured by Instron Inc.). Uniformly distributed load was applied to the rocks. This was ensured in all the tests by firstly having the specimen ends evenly polished, and secondly by using a hinge-type pedestal that adjusted the specimens centerline to fit perpendicularly to the loading platen and avoid misalignments. In all the tests, no additional friction-reducing layers in contact between the specimens and the loading platens were used. Thus, the platens, which were mirror-polished, were in direct contact with the specimens.

Fig. 1 shows the loading set-up used for testing the rock specimens. The closed-loop servo-controlled system of the compressive machine is fully digital, and is flexible to apply axial load by an inbuilt computer system as a function of controlling feedback signal: axial load, axial strain or lateral strain to provide sufficiently low rate.

Lateral-strain controlled method is the main method used here to study the post-peak characteristics of rocks. Thus, the applied axial load was controlled in a way keeping the lateral strain rate constant. In this sense, the electronic system and computer programme allowed the hydraulic system to be adjusted continuously and automatically to ensure the load to respond according to the feedback signal and the extent of damage to the specimen. Axial load (by a load cell), axial strain (by strain gauges, extensometers and external LVDTs) and lateral strain (by ring extensometers) were acquired continuously by a data acquisition system at a rate of 4 data points per second. To compare the results of lateral-strain controlled test with conventional testing methods by keeping constant axial loading and axial displacement rates, a few additional tests were performed.

3. Methods to control axial loading

Fig. 4 shows the time-histories of axial load, axial strain and lateral strain obtained after testing Hawkesbury sandstone
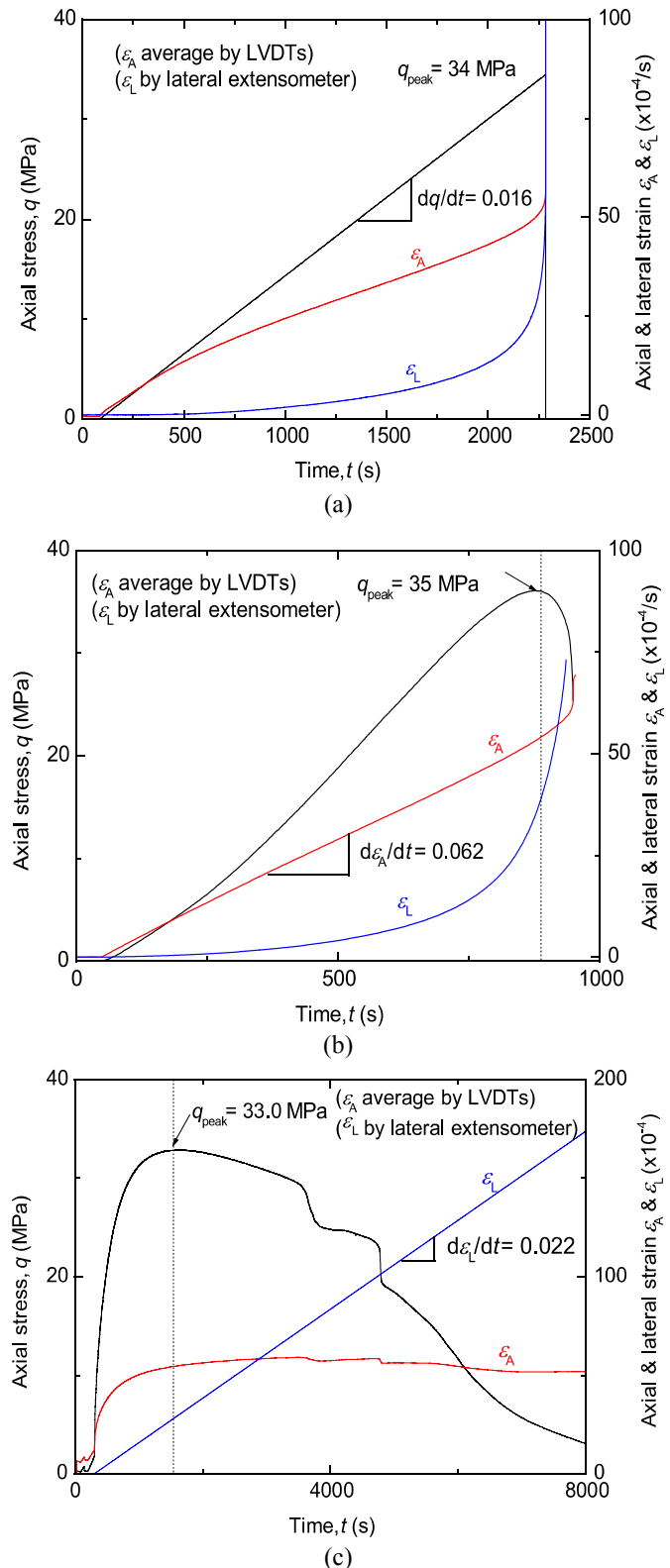

Fig. 4. Typical time-histories of loading and strains in uniaxial compression tests with (a) axial-load control feedback, (b) axial-strain control feedback, and (c) lateral-strain control feedback.

specimens under three different loading methods: (i) axial-load controlled (Fig. 4a); (ii) axial-strain controlled (Fig. 4b); and (iii) lateral-strain controlled (Fig. 4c). In this regard, axial-load controlled and axial-strain controlled methods were unable to

capture the complete post-peak stress–strain curves as Hawkesbury sandstone behaved at some moments as class II. On the other hand, lateral-strain controlled method was suitable to measure the complete post-peak response.

Fig. 5a, b and c shows the time-histories of axial load rate, axial strain rate and lateral strain rate for three loading methods described above, respectively. Axial load (or axial stress) rate, axial strain rate and lateral strain rate are given by finite increment of

load or strains with time as dF/dt (or dq/dt), $d\varepsilon_A/dt$ and $d\varepsilon_L/dt$, respectively. The axial stress is given in terms of q. The axial strain ε_A was obtained by the average reading of the external LVDTs, while ε_L came from the readings of lateral extensometer.

3.1. Axial-load controlled test

As shown in Fig. 4a, under constant axial load increment, i.e. 0.026 kN/s (or 0.016 MPa/s), initial axial and lateral strains increase gradually and then rapidly near the peak stress point. As it can be seen in Fig. 5a, in a load-controlled test, both axial and lateral strain rates increase dramatically as rock approaches the peak stress. The rock response was critical (i.e. a sharp reduction of the load-bearing capacity at constant displacement immediately after peak stress) and failure was eruptive. Following this method, the post-peak behaviour cannot be measured.

In the axial-load controlled test on Hawkesbury sandstone, axial strain rate at the beginning of the test was about 3×10^{-6} s^{-1}, and increased to 1×10^{-5} s^{-1} near the peak stress. This range of axial-strain rate satisfies static to quasi-static loading conditions in uni-axial compression tests for quasi-brittle materials (Wawersik and Fairhurst, 1970; Hudson et al., 1971; Wawersik and Brace, 1971; Bischoff and Perry, 1991).

3.2. Axial-strain controlled test

Fig. 4b shows the results of tests on Hawkesbury sandstone under constant axial strain increment of 6×10^{-6} s^{-1}, suitable to undertake quasi-static uniaxial compression test (Wawersik and Fairhurst, 1970; Hudson et al., 1971; Wawersik and Brace, 1971; Bischoff and Perry, 1991). The rest of the rock specimens tested with this method used axial strain rate of 6×10^{-6} s^{-1} as well. In this figure, as the stress is progressively reaching its maximum level, the lateral strain initially increases at a low rate and then becomes very high near the peak stress. As shown in Fig. 5b, at and after the peak stress, the lateral strain rate significantly increases. Generally speaking, if the specimen undergoes completely class I behaviour, the axial-strain controlled method can capture the post-peak stress and strain. For this specimen, the test was ended pre-maturely and only a small portion of post-peak stress–strain curve was captured until the moment when class II behaviour started dominating post-peak regime. Thereafter, the rock response was critical and the post-peak stress–strain behaviour was measured in compliance with the axial-strain controlled method.

3.3. Lateral-strain controlled tests

Figs. 4c and 5c show the results of tests on Hawkesbury sandstone under constant lateral strain increment of 2×10^{-6} s^{-1} (2×10^{-6} s^{-1} was used in all the lateral-strain controlled tests). As it can be seen in Fig. 5c, from the moment when the lateral-strain control takes over the test, at nearly the beginning of loading, the axial load rate and the axial strain rate were about 0.2 kN/s and 1.7×10^{-5} s^{-1}, respectively. Thereafter, they started to decrease gradually as the stress in the rock reached the peak stress. After the peak stress, the axial strain and axial load rate experienced fluctuations as the result of the strength response of the rock and the automatic adjustment of the applied load upon the damage extending in the specimen induced by the load. In other words, the post-peak regime was characterised by a gradual and progressive dropping with minor recoveries, if any, of the load-bearing capacity accompanied with crack development, and propagation.

During uniaxial compression, the complete portion of post-peak behaviour was captured straightforward using the lateral-strain
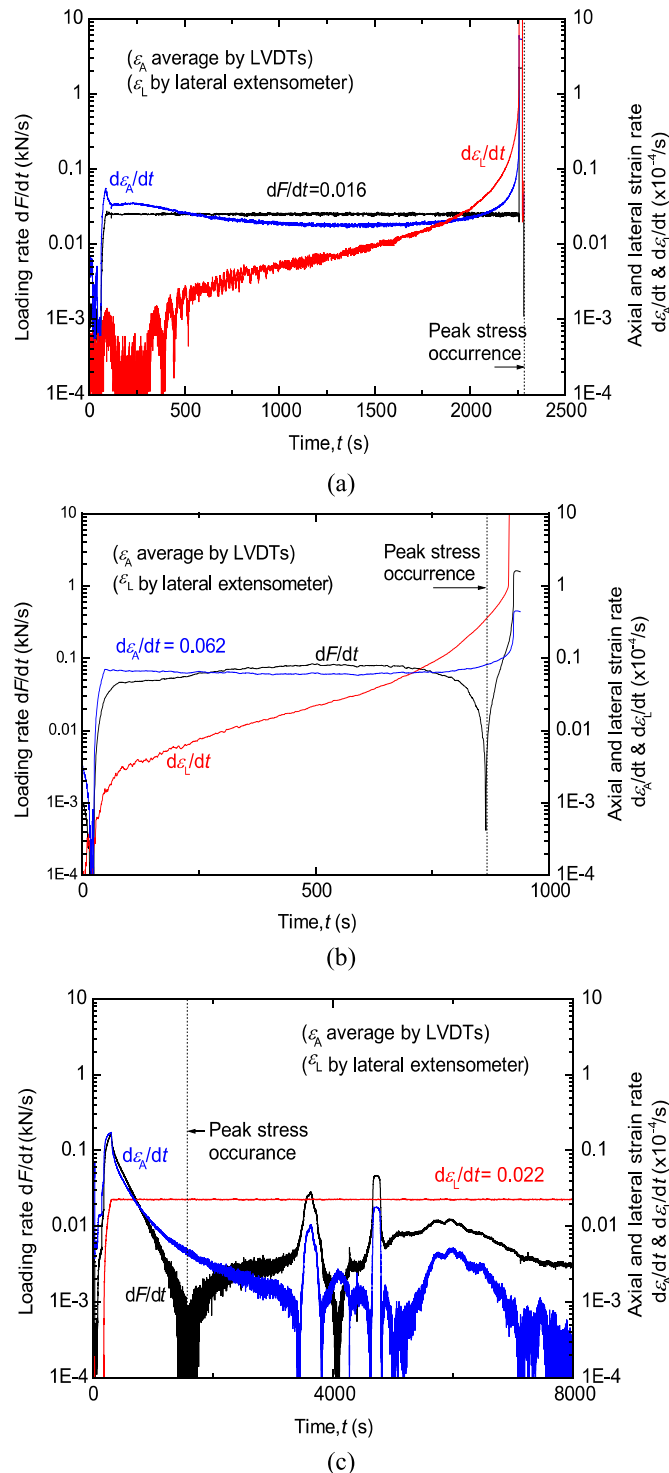

Fig. 5. Loading rate and strain rate in uniaxial compression with (a) axial load control feedback, (b) axial strain control feedback, and (c) lateral strain control feedback.

controlled method. The axial strain rate varied from 1.7×10^{-5} s^{-1} to 2×10^{-8} s^{-1} at the beginning until the end of the test with axial strain rate fluctuations. Axial strain rates satisfy static to quasi-static loading condition.

4. Result analyses and discussion

4.1. Pre-peak stress–strain characteristics

Fig. 6 shows the typical stress versus axial (ε_A), lateral (ε_L) and volumetric ($\varepsilon_{Vol} = \varepsilon_A + 2\varepsilon_L$) strains curves for Hawkesbury sandstone specimens with different aspect ratios, L/D, of 1.5, 2.4 and 3.5. In pre-peak regime, the characteristic threshold stresses for fracture damage associated with crack closure (q_{cc}), initiation (q_{ci}), and damage (q_{cd}) and peak stress (q_{peak}) were identified from the typical stress–strain curves of the rocks (Bieniawski, 1967; Martin and Chandler, 1994).

Table 1 summarises the average values of the peak stress q_{peak} (i.e. unconfined compressive strength, UCS), Young's modulus (E) and normalised crack damage stress q_{cd}/q_{peak} of Hawkesbury sandstone specimens having aspect ratios, L/D, of 1.5, 2.4 and 3.5. Young's modulus values were extracted from the linear-elastic portion of the stress–strain curves limited by q_{cc} and q_{ci}.

4.2. Post-peak strain field patterns and aspect ratio

Conventional strain measurement in material testing includes surface direct-contact bonded strain gauges. Local strain measurements by strain gauges (and extensometers) are insufficient to capture strains taking place around growing cracks and localised zones that occur in the post-peak regime. In this regard, strain gauge measurements are limited to a fixed gauge length and specific points of bonding, and they are damaged under large strains (i.e. commonly strains larger than 0.005). In this case, strain gauge damage makes the post-peak strains reading difficult or impossible. In general, 3D DIC overcomes these limitations. Nevertheless, internal deformation (i.e. strains and internal cracks development) within the specimens is not attainable by 3D DIC. Discussions on the stress–strain curves given herein are based on axial strains ε_A obtained from LVDTs, and strain patterns developing in the surface of the specimens are discussed based on DIC results.

In general, in all the rock specimens, it was observed that immediately after occurrence of the peak stress q_{peak}, progressive strength degradation took place accompanied with minor recovery of strength, until test was terminated long after the peak stress. The UCS values of the Hawkesbury sandstone specimens with aspect ratios, L/D, of 1.5, 2.4 and 3.5, on average, were 39 MPa, 35 MPa and 34 MPa, respectively, as shown in Table 1. The average values of Young's modulus were obtained to be 9.3 GPa, 9.7 GPa and 9.8 GPa, for aspect ratios, L/D, of 1.5, 2.4 and 3.5, respectively, as shown in Table 1. From these results, it is evident that the aspect ratio influences the peak stress values (i.e. peak stress increasing about 15%) and slightly influences the Young's modulus.

The above results may be mainly attributed to the effects of boundary restraint (i.e. a confinement zone) caused by frictional stresses between the specimens and loading platens (e.g. Kotsovos, 1983; van Vliet and van Mier, 1995, 1996). This is, in particular, more noticeable in the case of short specimens. In this view, in the case of specimens with L/D of 2.4 and 3.5, it is expected that a large part of the specimens (i.e. remote zones away from the influence of specimen-platens contact) is not significantly affected by the confinement effect due to frictional stresses taking place in specimen-platens contact area in contrast to short specimens with L/D of 1.5. This is because that specimens with lower L/D bear extensively the confinement effects of specimen-platens frictional
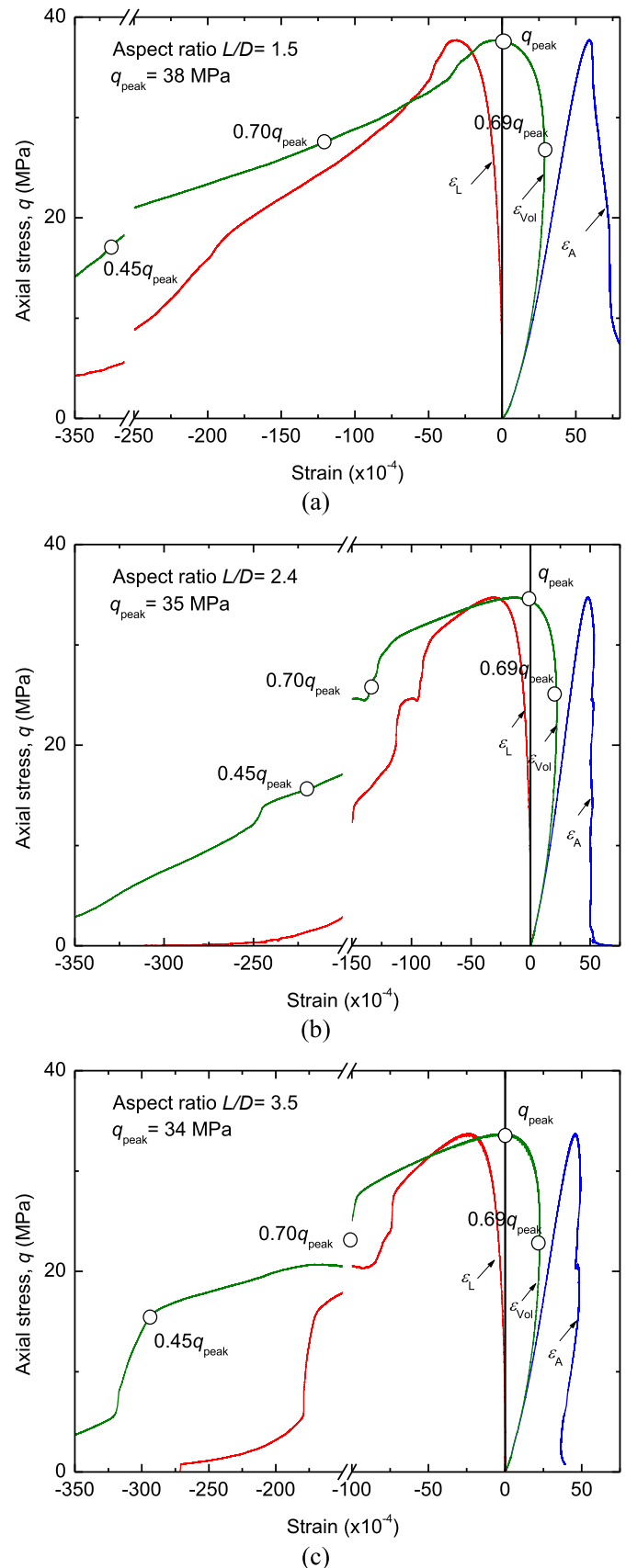

Fig. 6. Typical stress–strain curves of Hawkesbury sandstone specimens with aspect ratios L/D of (a) 1.5, (b) 2.4, and (c) 3.5.

Table 1
Average values of the peak stress, Young's modulus and normalised crack damage stress in the pre-peak regime stress–strain for Hawkesbury sandstone.

Number of tests	Aspect ratio	q_{peak} (MPa)	Young's modulus, E (GPa)	q_{cd}/q_{peak}
4	1.5	39 ± 1.7	9.3 ± 0.2	0.69 ± 0.06
4	2.4	35 ± 2	9.7 ± 0.3	0.69 ± 0.07
4	3.5	34 ± 2	9.8 ± 0.2	0.69 ± 0.05

stresses that are distributed within a influence zone that can include, if not the whole specimen, large parts of a short specimen. To examine the respective field of axial and lateral strains, four different key loading stages along the stress–strain curves were selected as shown in Fig. 6, that is, the crack damage stress q_{cd} (about $0.69q_{peak}$ in all the specimens, see Table 1), the peak stress q_{peak} in pre-peak regime and stresses at $0.7q_{peak}$ and $0.45q_{peak}$ in post-peak regime. In all the tests, no sign of perceptible major crack on the surface of the specimens was noticed either during pre-peak regime or at peak stress.

Figs. 7–9 show the fields of axial and lateral strains at the aforementioned selected stress levels. In the tests, due to the loading test method, strains growing on the surface of the specimens followed by rock failure process took place gradually. Therefore, there was not any issue in achieving strain measurement via 3D DIC technique in the post-peak regime until the end of the tests at a post-peak stress level of about $0.07q_{peak}$ (see the specimen conditions at the end of the tests in Fig. 3).

In general, the fields of axial and lateral strains within the area of interest suggest that the specimens deform more or less uniformly in pre-peak regime as shown by colour gradient in the specimens at stress levels of q_{cd} and q_{peak} in Figs. 7–9, i.e. nearly a single colour pattern in the specimens. Although some minor local contours of distinctive colour are seen in the specimens, it may be due to some local material inhomogeneity inherent of Hawkesbury sandstone and its deformation response. Conversely, in the post-peak regime, the colour patterns of axial and lateral strains in the surface of rock specimens are non-uniform. This is because in the post-peak regime, strains increase at different rates in the vicinity and outside the future failure plane. Strain field development in the surface of rock specimens suggests that strain starts localising progressively and develops at a lower rate in the pre-peak regime.

Axial splitting or faulting failure patterns in post-peak regime developed differently depending on the specimen aspect ratio as shown in Figs. 7–9. With short specimens having L/D of 1.5, only a small portion of the specimen (a zone at the mid-length of the specimen) is expected to be free from, or insignificantly affected by, any confinement effect due to specimen-platen frictional stresses, which is favourable for developing cracks. In other parts of the specimen, cracks development and propagation are likely to be arrested as the extent of confinement becomes more significant. Fig. 7 suggests that, for a short specimen, a reduced region where the confinement effect was lower, cracks were able to develop predominantly in the form of axial cracks (i.e. an axial splitting failure type). The short specimen prevented the formation of a predominant localised shear zone in contrast to specimens with L/D of 2.4 and 3.5.

On the other hand, when the specimens have aspect ratio values of 2.4 and 3.5 as shown in Figs. 8 and 9, a major cracking takes place in the form of a predominant single shear-failure plane (i.e. a faulting failure type). This may be due to the fact that large portions of the specimens are free from any confinement of specimen-platen frictional stresses, allowing enough room for strains to be localised.

Axial macro cracks, which extended in the direction of the axial load, were the typical characteristics of failure behaviours when L/D

was equal to 1.5. In this case, a sharp local unloading in the vicinity of the axial cracks in the rock surface took place in the post-peak regime, as shown by the distinctive spectrum of colour contours in Fig. 7a, i.e. reddish contours at post-peak stress levels of $0.7q_{peak}$ and $0.45q_{peak}$ (corresponding to local axial strains in the order of $0–0.001$) in contrast to greenish contours (corresponding to local axial strains of about $0.002–0.004$) obtained in pre-peak stress of $0.69q_{peak}$ and q_{peak}.

In the same manner, the total lateral deformation develops in compliance with constant lateral strain rate feedback, increasing gradually in pre- and post-peak regimes. However, in contrast to local lateral strain development in the pre-peak regimen, local lateral strains develop largely in post-peak regime within the vicinity of future axial cracks (local lateral strains in the order of $0.021–0.03$) of the specimen as shown by the greenish gradient colour in Fig. 7b at post-peak stress levels of $0.7q_{peak}$ and $0.45q_{peak}$.

It can be demonstrated by Figs. 8 and 9 that localisation around the future failure plane took place favourably for specimens with aspect ratios, L/D, of 2.4 and 3.5, in contrast to short specimens having L/D of 1.5. In this instance, the gradient of colours of the axial strain field, i.e. pink-bluish contours at post-peak stress levels of $0.70q_{peak}$ and $0.45q_{peak}$ in Figs. 8a and 9a, shows a major concentration of local axial strains in the vicinity and within the future failure plane (i.e. local axial strains in the order of $0.005–0.0075$) in contrast to local strains outside the future failure plane that experienced inelastic unloading (i.e. local axial strains in the order of $0.0025–0.004$) depicted by a predominant greenish colour contour.

In a similar manner, the total lateral deformation develops gradually in compliance with constant lateral strain rate feedback. However, local lateral strains develop at different extents in the specimens. As shown by the green-to-red colour pattern of the field of lateral strains in Figs. 8b and 9b, large lateral strains took place in the vicinity and within the future failure plane (corresponding to strains in the order of 0.009 to greater than 0.045) for post-peak stress levels of $0.7q_{peak}$ and $0.45q_{peak}$. In contrast, local lateral strains that took place either in the entire area of interest during pre-peak regime or outside the future failure plane during post-peak regime were plotted by a predominant pinkish colour contour (corresponding to strains in the range of $0–0.006$).

Furthermore, the patterns of strains of specimens with L/D of 2.4 and 3.5 indicated that the inclination of the shear band seemed to be more or less constant once the shear band was initiated.

Fig. 10 shows the normalised axial stress–strain curves for specimens with L/D of 1.5, 2.4 and 3.5. The axial stress–strain curves were normalised by dividing the stresses and strains by the peak stress and the axial strain at peak stress of their respective L/D values. This figure emphasises the dependence of the post-peak stress–strain characteristics, obtained under the same testing conditions, on specimen height. The degree of confinement by frictional stresses on the specimens influenced the characteristics of cracks development in the specimens and, therefore, the shape of the post-peak stress–strain curves.

The curves in Fig. 10, in general, show that rock brittleness increases with an increase in the specimen aspect ratio, if the brittleness is defined by the characteristics of the axial stress–strain post-peak curve and post-peak stiffness (i.e. the slope of axial stress–strain relation). Nonetheless, specimens with $L/D = 2.4$ and 3.5 almost demonstrated similar brittleness and post-peak responses.

Post-peak stress–strain curves showed that specimens with $L/D = 1.5$ predominantly followed a class I rock behaviour throughout the loading test. On the other hand, specimens with $L/D = 2.4$ and 3.5 showed a combination of classes I and II behaviours. Therefore, the extent of external confinement in the specimens, due to specimen-platens frictional stresses, may have
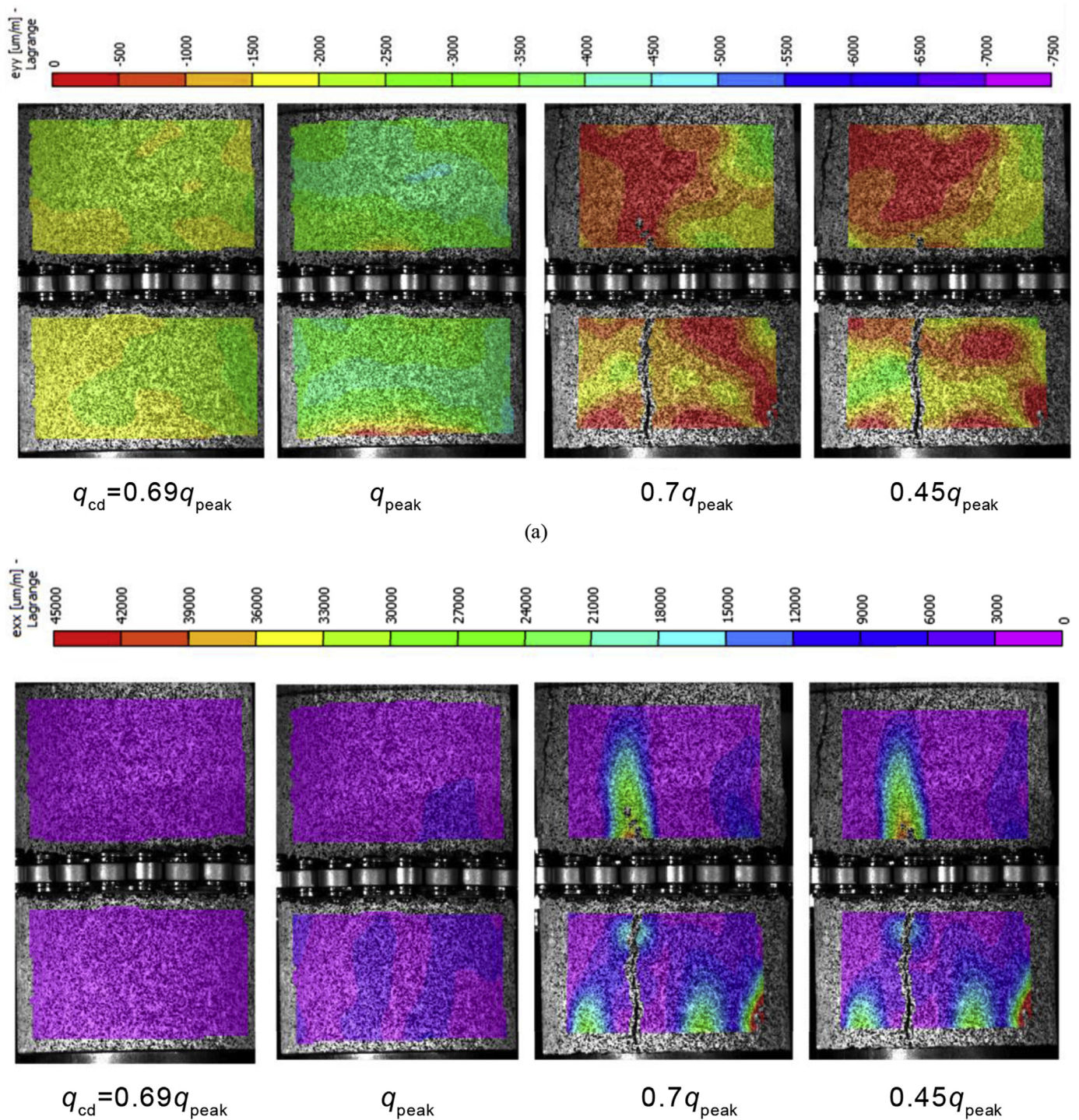
Fig. 7. Fields of (a) axial and (b) lateral strains in Hawkesbury sandstone ($L/D = 1.5$) developed in pre-peak regime ($0.69q_{peak}$ and q_{peak}) and post-peak regime ($0.7q_{peak}$ and $0.45q_{peak}$).

played a significant role in the failure pattern and therefore in the stress−strain response.

The pre-peak curves in Fig. 10 for different aspect ratios fall into a unique curve irrespective of the specimen height when L/D is 2.4 and 3.5, unlike the curves attributed to specimens with L/D of 1.5. Nonetheless, the deviation of pre-peak stress−strain curves for specimens with L/D of 2.4, 3.5 and 1.5 is not significant. In pre-peak regime, it is expected to obtain a single normalised stress−strain curve, with the peak stress independent of the specimen length, if

the specimen-platens frictional stress is eliminated completely by an effective friction-reduction layer inserted between the specimens and the loading platens. Nevertheless, even under low frictional stress conditions, post-peak curves may be sensitive to specimen length (van Vliet and van Mier, 1995). However, the present study shows that the specimen-platens frictional stress is almost negligible when L/D is equal to or greater than 2.4. For rock specimens having L/D of 2.4 and 3.5, the Young's modulus (i.e. 9.7 GPa and 9.8 GPa, respectively), crack damage stress ratio (i.e.
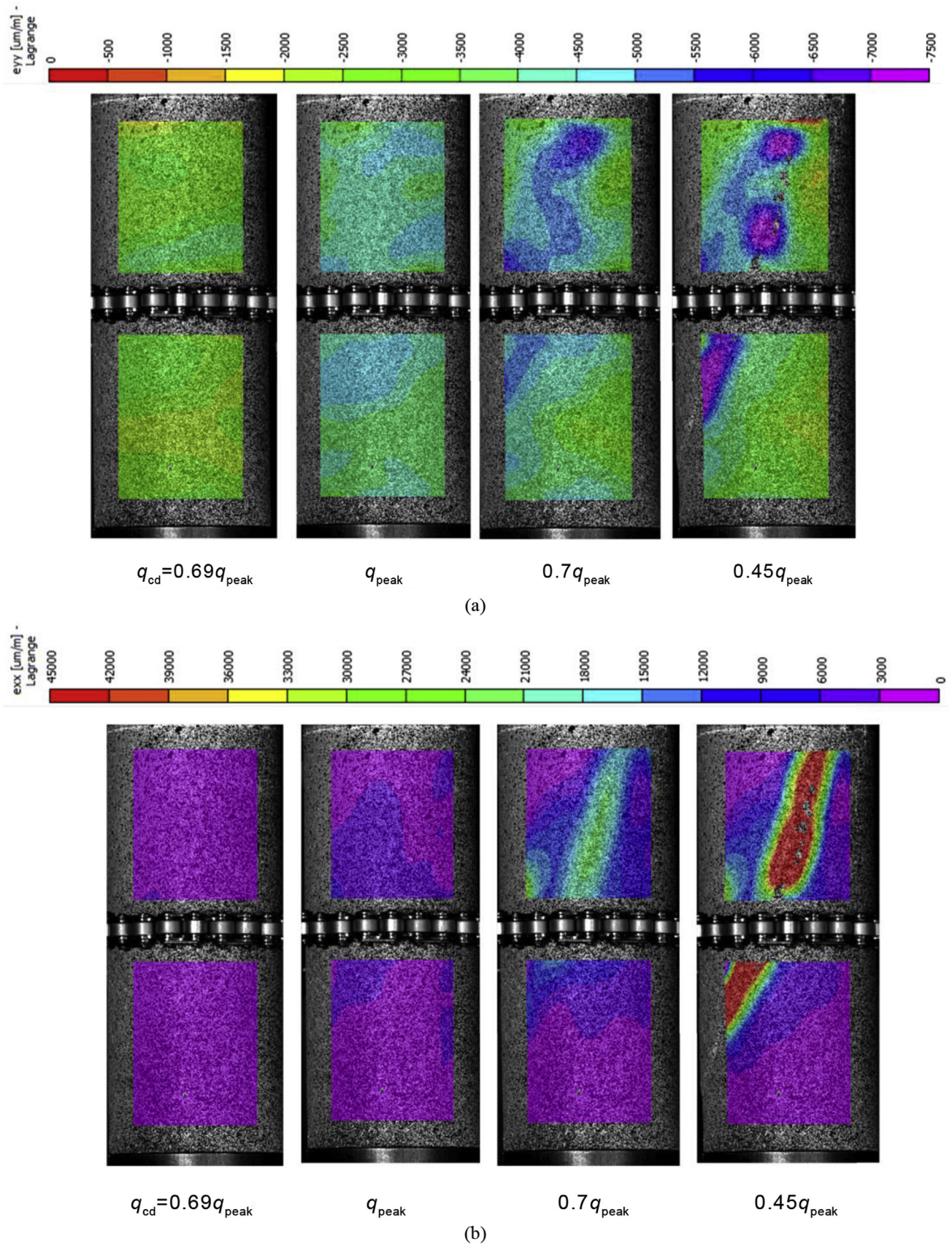
Fig. 8. Fields of (a) axial and (b) lateral strains in Hawkesbury sandstone ($L/D = 2.4$) developed in pre-peak regime ($0.69q_{peak}$ and q_{peak}) and post-peak regime ($0.7q_{peak}$ and $0.45q_{peak}$).
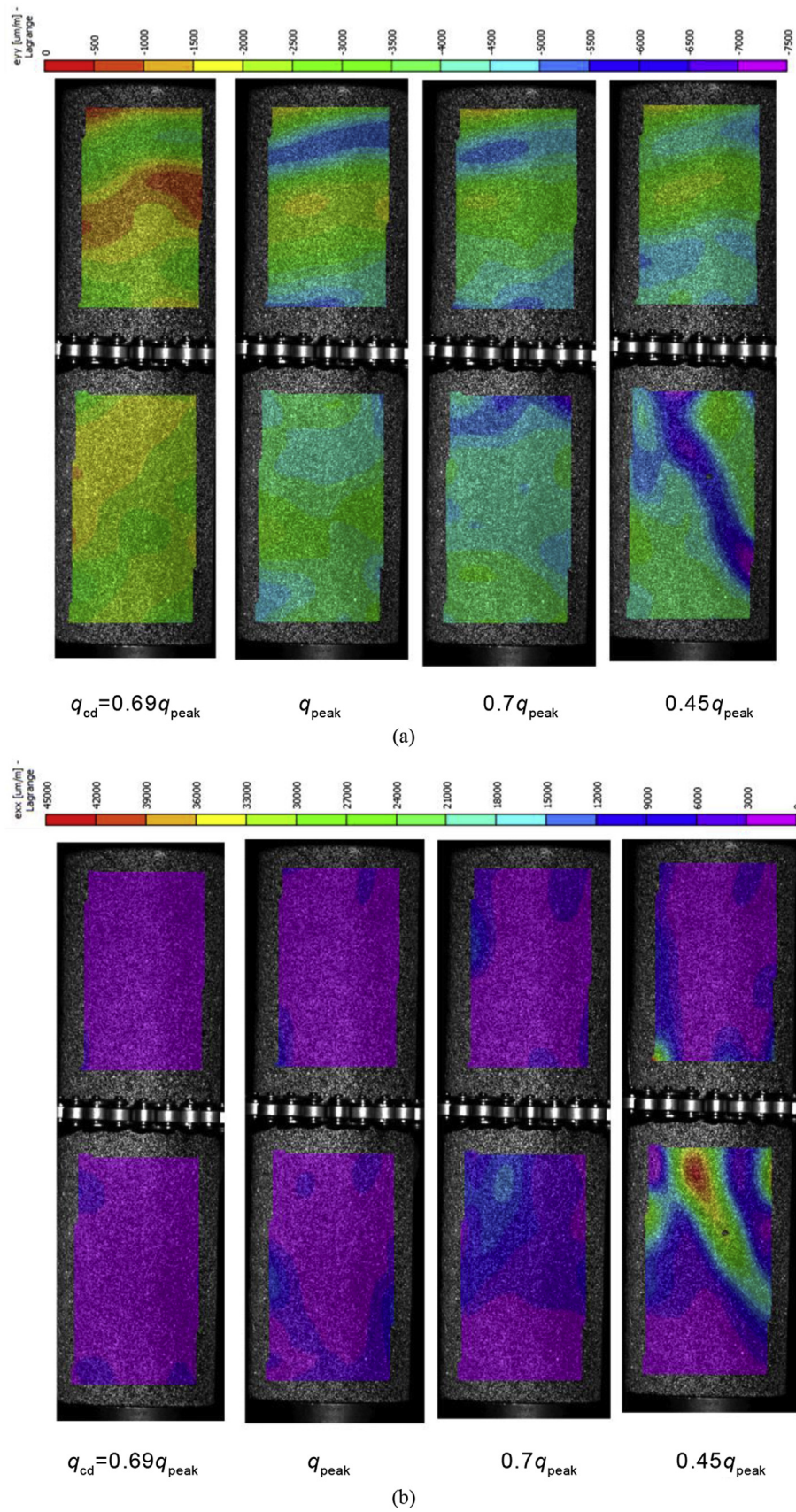
Fig. 9. Fields of (a) axial and (b) lateral strains in Hawkesbury sandstone ($L/D = 3.5$) developed in pre-peak regime ($0.69q_{peak}$ and q_{peak}) and post-peak regime ($0.7q_{peak}$ and $0.45q_{peak}$).
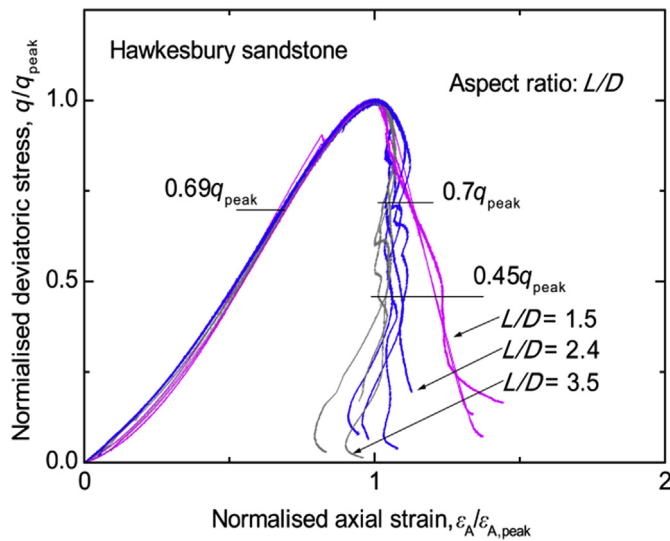
Fig. 10. Normalised stress–strain curves of Hawkesbury sandstone with aspect ratios, L/D, of 1.5, 2.4 and 3.5; $\varepsilon_{A,\,peak}$ is the axial strain at peak stress.

0.69) and peak stress (i.e. 35 MPa and 34 MPa, respectively) were nearly the same (see Table 1), and the post-peak stress–strain curves nearly overlapped each other (see Fig. 10). In addition, the predominant single shear-failure and strain localisation patterns taking place in the surface of the specimens (see Figs. 8 and 9) were almost identical. Therefore, it can be concluded that as far as the aspect ratio is in the range of 2.4–3.5, in the test conditions of the present study, the confinement effect due to frictional stresses on the pre- and post-peak stress–strain characteristic parameters of the rock is negligible.

5. Conclusions

Post-peak stress–strain characteristics and strain patterns of Hawkesbury sandstone were studied under quasi-static loading in uniaxial compression tests. Unlike lateral-strain controlled tests, the typical axial-load controlled or axial-strain controlled test methods were unable to capture the complete post-peak stress–strain behaviour of the rock as Hawkesbury sandstone behaves following a combination of classes I and II behaviours. Axial-load controlled method can only measure pre-peak stress–strain behaviour and axial-strain controlled method, provided sufficiently low rate and monotonic strain increase, can capture post-peak curves only if rock completely follows class I behaviour. This outcome demonstrates that an apparent post-peak stress–strain class I behaviour with sudden critical stress reduction to zero may be due to the method adopted to control axial load and not necessarily material behaviour.

Post-peak stress–strain characteristics and strain patterns development of sandstone specimens having different aspect ratios were examined by applying 3D DIC technique. DIC technique allowed mapping the development of strains in the specimens throughout the compression tests. The peak stress, the post-peak stress–strain relations, the characteristics of post-peak localisation and the field strain patterns development, were affected at different extents by aspect ratios. This may be mainly attributed to the effects of boundary restraint caused by frictional stresses between the specimens and loading platens affecting large parts of short specimens, and being less significant for slender specimens. It was found that short specimens prevented shear zone localisation to occur, and axial macro cracks extending in the direction of the

axial load were observed at the end of the compression tests. Progressive localisation around the future failure plane favourable to shear zone localisation took place for specimens typically with aspect ratios of 2.4 and 3.5. In addition, it was found that for specimens with aspect ratios of 2.4 or 3.5, the pre- and post-peak stress–strain characteristics, including strain localisation patterns, were almost identical. Therefore, it seems that the effect of specimen-platens frictional stress becomes negligible on the stress–strain characteristics of rock when the aspect ratio of specimen is greater than 2.4.

Conflict of interest

The authors wish to confirm that there are no known conflicts of interest associated with this publication and there has been no significant financial support for this work that could have influenced its outcome.

Acknowledgement

References

Bieniawski ZT. Mechanism of brittle fracture of rock: Part I—theory of the fracture process. International Journal of Rock Mechanics and Mining Sciences & Geomechanics Abstracts 1967;4(4):395–406.

Bieniawski ZT, Bernede MJ. Suggested methods for determining the uniaxial compressive strength and deformability of rock materials: Part 1. Suggested method for determination of the uniaxial compressive strength of rock materials. International Journal of Rock Mechanics and Mining Sciences & Geomechanics Abstracts 1979;16(2):137–8.

Bischoff PH, Perry SH. Compressive behaviour of concrete at high strain rates. Materials and Structures 1991;24(6):425–50.

Dautriat J, Bornert M, Gland N, Dimanov A, Raphanel J. Localized deformation induced by heterogeneities in porous carbonate analysed by multi-scale digital image correlation. Tectonophysics 2011;503(1–2):100–16.

Fairhurst CE, Hudson JA. Draft ISRM suggested method for the complete stress-strain curve for intact rock in uniaxial compression. International Journal of Rock Mechanics and Mining Sciences 1999;36(3):279–89.

Gowd TN, Rummel F. Effect of confining pressure on the fracture behaviour of a porous rock. International Journal of Rock Mechanics and Mining Sciences & Geomechanics Abstracts 1980;17(4):225–9.

Hawkes I, Mellor M. Uniaxial testing in rock mechanics laboratories. Engineering Geology 1970;4(3):179–285.

Hudson JA, Brown ET, Fairhurst C. Optimizing the control of rock failure in servo-controlled laboratory tests. Rock Mechanics 1971;3(4):217–24.

ISRM. Rock characterization testing and monitoring—ISRM suggested methods. Oxford: Pergamon; 1981.

Kotsovos MD. Effect of testing techniques on the post-ultimate behaviour of concrete in compression. Matériaux et Construction 1983;16(1):3–12.

Kumar R, Sharma KG, Varadarajan A. Post-peak response of some metamorphic rocks of India under high confining pressures. International Journal of Rock Mechanics and Mining Sciences 2010;47(8):1357–62.

Labuz JF, Biolzi L. Experiments with rock: remarks on strength and stability issues. International Journal of Rock Mechanics and Mining Sciences 2007;44(4):525–37.

Martin CD, Chandler NA. The progressive fracture of Lac du Bonnet granite. International Journal of Rock Mechanics and Mining Sciences & Geomechanics Abstracts 1994;31(6):643–59.

Munoz H, Taheri A, Chanda EK. Fracture energy-based brittleness index development and brittleness quantification by pre-peak strength parameters in rock uniaxial compression. Rock Mechanics and Rock Engineering 2016a;49(12):4587–606.

Munoz H, Taheri A, Chanda EK. Pre-Peak and post-peak rock strain characteristics during uniaxial compression by 3D digital image correlation. Rock Mechanics and Rock Engineering 2016b;49(7):2541–54.

Nguyen TL, Hall SA, Vacher P, Viggiani G. Fracture mechanisms in soft rock: identification and quantification of evolving displacement discontinuities by extended digital image correlation. Tectonophysics 2011;503(1–2):117–28.

Sutton MA, Orteu JJ, Schreier HW. Image correlation for shape, motion and deformation measurements: basic concepts, theory and applications. Springer, LLC; 2009.

Taheri A, Tani K. Use of down-hole triaxial apparatus to estimate the mechanical properties of heterogeneous mudstone. International Journal of Rock Mechanics and Mining Sciences 2008;45(8):1390–402.

Taheri A, Yfantidis N, Olivares CL, Connelly BJ, Bastian TJ. Experimental study on degradation of mechanical properties of sandstone under different cyclic loadings. Geotechnical Testing Journal 2016;39(4):673–87.

van Vliet MRA, van Mier JGM. Softening behaviour of concrete under uniaxial compression. In: Wittmann FH, editor. Fracture Mechanics of Concrete Structures, Proceedings FRAMCOS-2. Freiburg: AEDIFICATIO Publishers; 1995. p. 383–96.

van Vliet MRA, van Mier JGM. Experimental investigation of concrete fracture under uniaxial compression. Mechanics of Cohesive-frictional Materials 1996;1(1):115–27.

Wawersik WR, Fairhurst C. A study of brittle rock fracture in laboratory compression experiments. International Journal of Rock Mechanics and Mining Sciences & Geomechanics Abstracts 1970;7(5):561–75.

Wawersik WR, Brace WF. Post-failure behavior of a granite and diabase. Rock Mechanics 1971;3(2):61–85.

Zheng H, Liu DF, Lee CF, Ge XR. Principle of analysis of brittle-plastic rock mass. International Journal of Solids and Structures 2005;42(1):139–58.

Dr. Henry Munoz is currently a Post-Doctoral fellow at the Institute of Industrial Science of the University of Tokyo (Japan). He received his PhD from the University of Adelaide (Australia) with a Dean's Commendation for research and MEng (research) from Tokyo University of Science (Japan). He previously worked as a research intern/member at Deep Exploration Technologies CRC (Australia), CSIRO (Australia), Railway Technical Research Institute (Japan), PRS Mediterranean (Israel) and Public Works Research Institute (Japan).